Supporting Information for Emergent magnetic state in (111)-oriented quasi-two-dimensional spinel oxides

Xiaoran Liu,[*,†] Sobhit Singh,[†] Brian J. Kirby,[‡] Zhicheng Zhong,[¶] Yanwei Cao,[¶] Banabir Pal,[†] Mikhail Kareev,[†] Srimanta Middey,[§] John W. Freeland,[‖] Padraic Shafer,[⊥] Elke Arenholz,[⊥] David Vanderbilt,[†] and Jak Chakhalian[†]

†*Department of Physics and Astronomy, Rutgers University, Piscataway, New Jersey 08854, USA*

‡*NIST Center for Neutron Research, National Institute of Standards and Technology, Gaithersburg, Maryland 20899, USA*

¶*Ningbo Institute of Materials Technology and Engineering, Chinese Academy of Sciences, Ningbo, Zhejiang 315201, China*

§*Department of Physics, Indian Institute of Science, Bengaluru 560012, India*

‖*Advanced Photon Source, Argonne National Laboratory, Argonne, Illinois 60439, USA*

⊥*Advanced Light Source, Lawrence Berkley National Laboratory, Berkeley, California 94720, USA*

E-mail: xiaoran.liu@rutgers.edu

PNR Fitting

The PNR experiments were performed at the PBR beamline at the NIST Center for Neutron Research. Samples were field-cooled and measured in a magnetic field H = 700 mT applied in the plane of the sample surface. The polarized beam was incident on the sample at a grazing angle, and the specular reflectivity was recorded as a function of wave vector transfer Q_z along the surface normal. The depth profiles of the nuclear scattering length density (nSLD) and the magnetization (M) component parallel to H were deduced via fitting the non-spin-flip curves to a superlattice model, in which the thickness and roughness of each layer was already determined through X-ray reflectivity, as published elsewhere,[1] and therefore fixed during the fit. The error bars of the best fit parameters represent 95% confidential interval.

In addition to the data taken at 5 K displayed in the main text, PNR measurements were also performed on the ultra-thin $[(CoCr_2O_4)_n/(Al_2O_3)_2]_N$ superlattices at different temperatures. These results, together with fittings are shown in Fig. S1. The estimated net magnetization of n = 2 is (0.33±0.08) μ_B/f.u. at 10 K, close to the value of ∼0.33 μ_B/f.u. obtained at 5 K. Moreover, the estimated net magnetization of n = 4 is (0.39±0.09) μ_B/f.u. at 20 K, also close to the value of ∼0.40 μ_B/f.u. obtained at 5 K. These results indicate the in-plane magnetization of each superlattice is almost saturated after field-cooling in 700 mT field down to the base temperature.

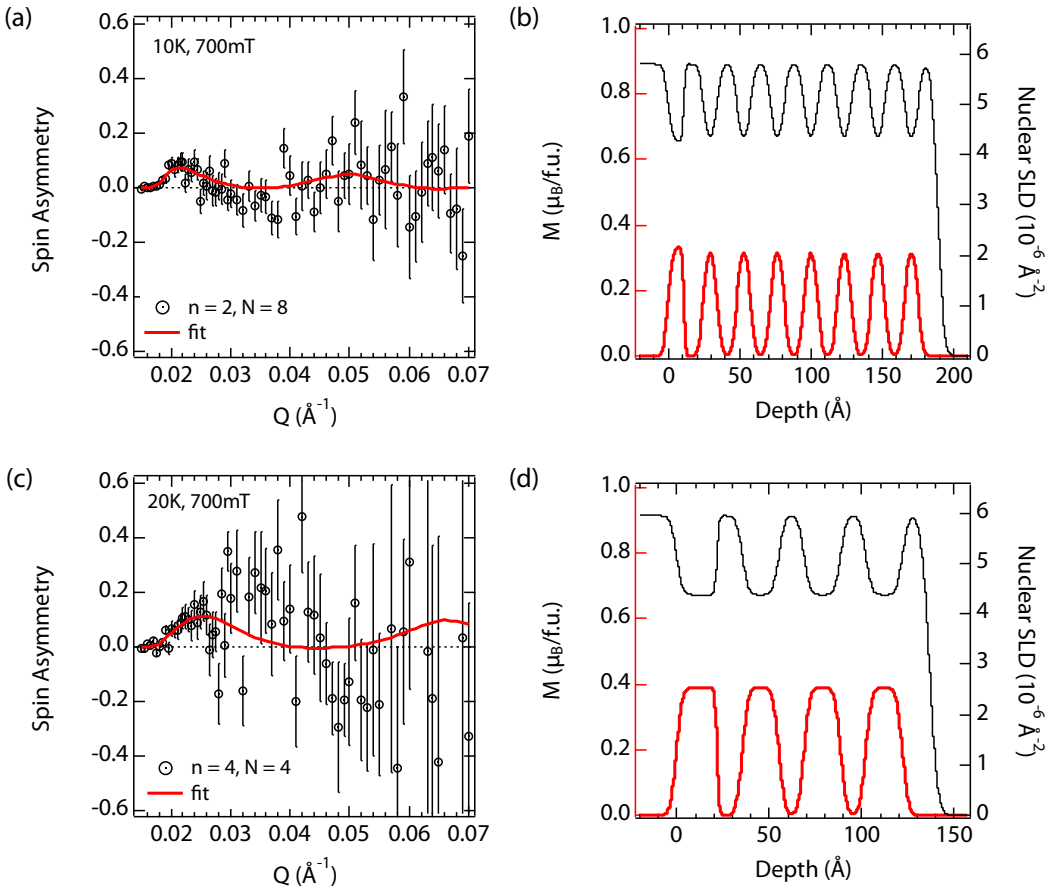

Figure S1: (a)-(b) Spin asymmetry and the depth profile of $[(CoCr_2O_4)_n/(Al_2O_3)_2]_N$ (n = 2, N = 8) at 10 K. The net magnetization per $CoCr_2O_4$ is estimated ∼0.33 μ_B/f.u. (c) and (d) Spin asymmetry and the depth profile of $[CoCr_2O_4)_n/(Al_2O_3)_2]_N$ (n = 4, N = 4) at 20 K. The net magnetization per $CoCr_2O_4$ is estimated ∼0.39 μ_B/f.u.

XMCD Sum Rules Analyses

XMCD sum-rules[2,3] were applied on the spectra of both Co and Cr $L_{2,3}$ edges. Specifically, since the L_3 and L_2 edges are well separated, the spin and orbital magnetic moment of Co was deduced according to the following equations:

$$m_{\text{orbital}} = -\frac{4q}{3r} \times (10 - n_d) \tag{1a}$$

$$m_{\text{spin}} = -\frac{6p - 4q}{r} \times (10 - n_d) \tag{1b}$$

On the other hand, due to the spectral overlap of L_3 and L_2 edges of Cr, while the orbital sum rule is not affected, application of the spin sum rule on Cr should be modified by the so-called "spin correction factor (SC)":[4,5]

$$m_{\text{spin}} = -\frac{6p - 4q}{r} \times (10 - n_d) \times SC \tag{2}$$

The detailed process of how to extract SC from the spectra was reported by E. Goering.[6] In above equations, r, p, and q represents the three integrals over XAS and XMCD spectra,[7] as shown on Fig. S2. Note, the XAS in each figure is the white-line intensity after subtracting the edge-jump background. n_d represents the number of electrons on the d levels. In this case, $n_d = 3$ for Cr^{3+} ($3d^3$) and 7 for Co^{2+} ($3d^7$). The magnetic dipole term $\langle T_z \rangle$, which can give an error of $\sim 10\%$ in the estimation of the spin moment is omitted for convenience. In Table S1, we summarized the obtained values of SC and magnetic moment of each ion, and the net magnetization of $CoCr_2O_4$ per formula unit (f.u.).

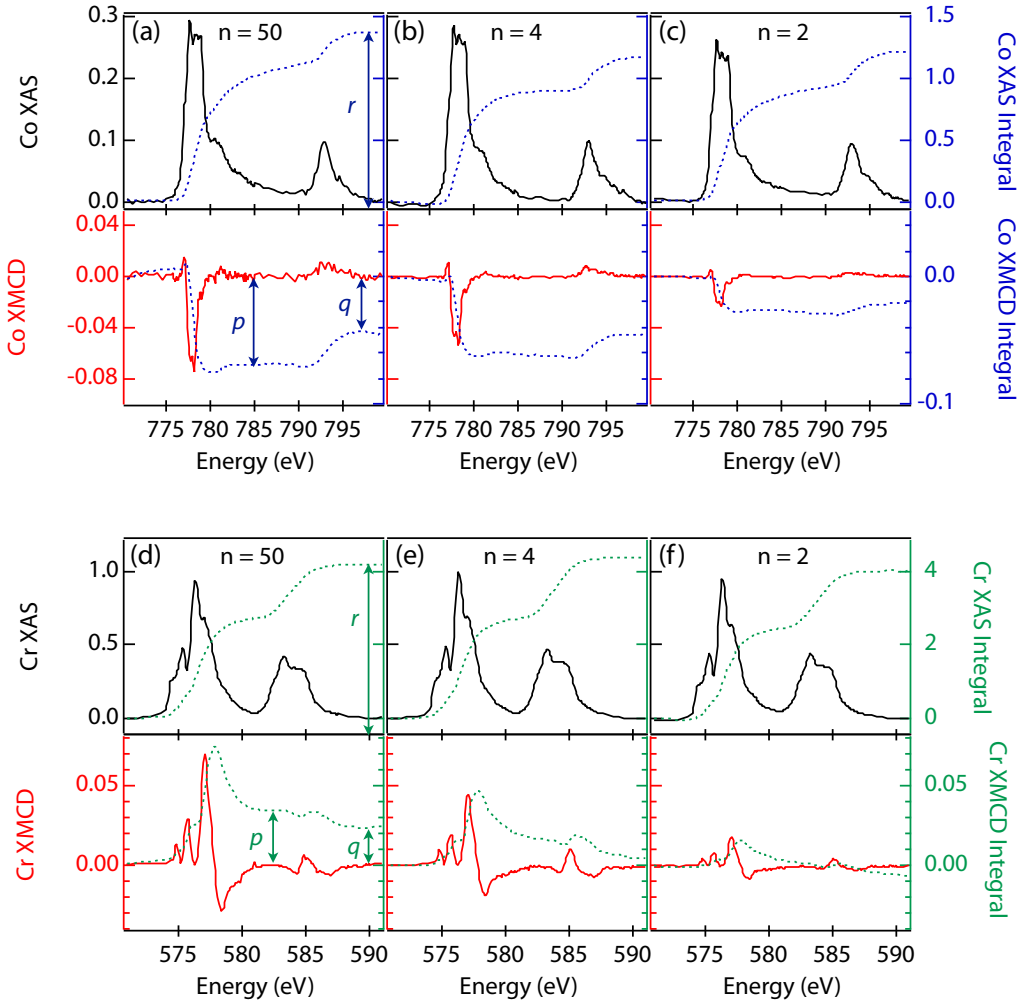

Figure S2: Sum-rules analyses of the XMCD spectra taken around the Co (a)-(c) and the Cr (d)-(f) $L_{2,3}$ edges from both the bulk-like ($n = 50$) $CoCr_2O_4$ and the ultra-thin $(CoCr_2O_4)_n/(Al_2O_3)_2$ ($n = 4$ and 2), respectively. The left-axis represents the spectrum and the right-axis represents the integral over the corresponding spectrum.

Table S1: Values of SC, magnetic moment of each element (Co^{2+} and Cr^{3+}) of each ion, and the net magnetization of $CoCr_2O_4$.The net moment per $CoCr_2O_4$ formula unit (f.u.) is calculated as $m_{\mathrm{net}} = (m_{\mathrm{Co}} + 2m_{\mathrm{Cr}})/cos30^{\circ}$, where a factor of $cos30^{\circ}$ is included to account for the incident angle of x-rays.

n (QL)	$\mathrm{SC_{Cr}}$	$m_{\mathrm{s,Cr}}$ (μ_B)	$m_{\mathrm{o,Cr}}$ (μ_B)	m_{Cr} (μ_B)	$m_{\mathrm{s,Co}}$ (μ_B)	$m_{\mathrm{o,Co}}$ (μ_B)	m_{Co} (μ_B)	m_{net} (μ_B/f.u.)
50	1.2	-0.23	-0.05	-0.28	0.53	0.12	0.65	0.10
4	1.5	-0.21	-0.01	-0.22	0.49	0.15	0.64	0.23
2	1.5	-0.087	0.013	-0.074	0.19	0.069	0.26	0.13

Brillouin Function Fitting

For $n = 4$ and 2, the field-dependent XMCD curves can be well reproduced using a two-sublattice ferrimagnetic model.[8–10] In this model, for a normal spinel structure, the net magnetic moments of each sublattice i (here i = Co, Cr) below the Curie temperature are antiparallel. Within the nearest neighbor approximation, the Weiss molecular field on each site is composed of both the inter-sublattice ($J_{\text{Co-Cr}}$) and the intra-sublattice ($J_{\text{Co-Co}}$ and $J_{\text{Cr-Cr}}$) exchange interactions.

For each sublattice below the transition temperature, the net magnetization per site is given by the modified Brillouin function:

$$y_i = B_{S_i}(x_i) = \frac{2S_i+1}{2S_i} coth(\frac{2S_i+1}{2S_i}x_i) - \frac{1}{2S_i} coth(\frac{1}{2S_i}x_i) \tag{3}$$

with

$$y_i = M_i/M_{i0} \tag{4}$$

$$x_i = \frac{g_i \mu_B S_i}{k_B T}[H + w(-a_i M_i - M_j)], i \neq j \tag{5}$$

in which M_i is the magnetization per site of the ith sublattice, and M_{i0} is the saturated magnetization. Therefore y_i is the reduced magnetization. S_i is the spin magnetic moment of the ith sublattice. In this case, Co^{2+} and Cr^{3+} ions have equal values, $S_{Co} = S_{Cr} = 3/2$. g_i is the gyromagnetic ratio and we took $g_{Co} = 2.2$ and $g_{Cr} = 2.0$.[11] w in x_i represents the inter-sublattice Weiss constant, which is linearly proportional to the inter-sublattice exchange interaction $J_{\text{Co-Cr}}$. And a_i is the factor expressing the intensity of the intra-sublattice exchange interaction with respect to the inter-sublattice value. By fitting the experimental data using this modified Brillouin function, the strength of the exchange interactions can be estimated.[12–14]

In order to relate the variables to our XMCD results, we rewrite x_i into the normalized

form:

$$x_i = \frac{g_i \mu_B S_i H}{k_B T} + \theta \cdot \frac{3S}{S+1}(-a_i \frac{M_i}{M_{i0}} - \frac{M_j}{M_{j0}}), i \neq j \tag{6}$$

$$\theta = \frac{g_i^2 \mu_B^2 S(S+1)}{3 k_B T} w \tag{7}$$

Now M_i is the field-dependent XMCD intensity. Taking the non-saturation effect into consideration, we denote a ratio $C_i \equiv M_{i0}/M_{i,H=0.5T}$ where $M_{i,H=0.5T}$ is the XMCD intensity measured under 0.5 T external field. Finally, the ferrimagnetic Brillouin function has the form:

$$y_i = \frac{M_i}{C_i \cdot M_{i,H=0.5T}} = B_{S_i}(x_i) \tag{8}$$

$$x_i = \frac{g_i \mu_B S_i H}{k_B T} + \theta \cdot \frac{3S}{S+1} \cdot \frac{1}{C_i}(-a_i \frac{M_i}{M_{i,H=0.5T}} - \frac{M_j}{M_{i,H=0.5T}}), i \neq j \tag{9}$$

The fitting parameters are the dimensionless C_i, θ, and a_i. Especially, in our case, a_{Co} is negligible due to the weak exchange interaction J_{AA} between nearest neighbor Co sites. For $n = 4$, we obtained $C_{Co} = 2.54 \pm 0.10$, $C_{Cr} = -2.11 \pm 0.01$; $\theta = 1.28 \pm 0.01$, and $a_{Cr} = 0.49 \pm 0.01$. For $n = 2$, $C_{Co} = 4.03 \pm 0.28$, $C_{Cr} = -1.67 \pm 0.07$; $\theta = 1.17 \pm 0.01$, and $a_{Cr} = 0.37 \pm 0.01$.

Determination of Spin Correlation Length

Here, we show that the inert Al_2O_3 spacer is thick enough so that the periodic $CoCr_2O_4$ slabs are magnetically noninteracting and are well-isolated from each other. It is known that as the thickness (t) of a magnetic material is reduced comparable to its spin-spin correlation length, the magnetic ordering temperature (T_C) shifts towards lower temperatures. The scaling relationship between T_C and t is given by,[15]

$$T_C(t) = T_C(bulk)\left[1 - (\frac{\xi_0}{t})^{\lambda}\right], \tag{10}$$

where $T_C(bulk)$ is the transition temperature in bulk, λ is a shift exponent, and ξ_0 is the characteristic spin-spin correlation length. Fig. S3 shows the fitting of the above equation to our data. Based on the fit we obtain a spin-spin correlation length ξ_0 ~0.60 nm. Note that the thickness of Al_2O_3 spacer is 1.3 nm, thus, it ensures that the alternating $CoCr_2O_4$ slabs are magnetically non-interacting.

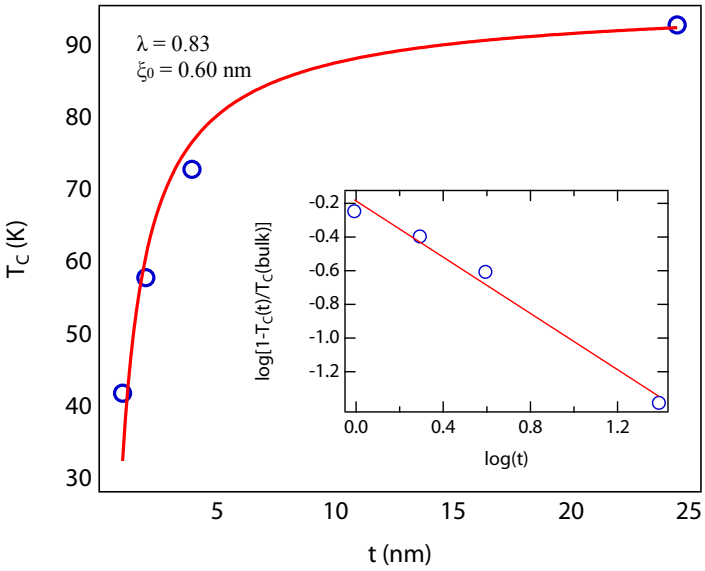

Figure S3: Scaling relation between Curie temperature T_C and slab thickness t of $CoCr_2O_4$. The spin-spin correlation length ξ_0 is extracted from the fit.

Density Functional Theory Calculations

Computational details

The first-principles Density Functional Theory (DFT) calculations were performed within the projected-augmented wave (PAW) framework[16,17] using the Vienna *ab initio* simulation package (VASP).[18,19] We considered nine valence electron of Co ($3d^7 4s^2$), twelve valence electrons of Cr ($3p^6 3d^5 4s^1$), and six valence electrons of O ($2s^2 2p^4$) in the PAW pseudo-potentials. The Perdew-Burke-Ernzerhof (PBE)[20] parametrized generalized gradient approximation was used to compute the exchange-correlation energy. A $8 \times 8 \times 8$ Monkhorst-Pack k-mesh was used to sample the Brillouin zone, and 600 eV was used as the cutoff for plane waves. The structures were optimized until the residual forces were less than 10^{-3} eV/Å, and 10^{-8} eV was used as the convergence criterion for total energy in the self-consistent DFT calculations. The PBE+U scheme was employed for the treatment of strongly correlated $3d$ orbitals at the mean-field level (Dudarev's approach[21]). We set $U_{Co} = 3.3$ eV and $U_{Cr} = 3.7$ eV for the on-site Hubbard interaction terms for the d electrons of Co and Cr. These values are reported to correctly describe the structural phase transitions and the magnetic structure of $CoCr_2O_4$.[22–25] Using the above parameters, a Néel-type magnetic configuration (all Co ↑, and all Cr ↓) was obtained as the lowest energy magnetic configuration for bulk $CoCr_2O_4$, where the total magnetic moment of Co and Cr atoms stayed around $2.7\,\mu_B$ and $3.0\,\mu_B$, respectively. The optimized lattice parameters of cubic spinel structure (space group $Fd\bar{3}m$) of $CoCr_2O_4$ are $a = b = c = 8.34$ Å, with $x = 0.26$ as an internal structural parameter for oxygen atoms.

To simulate the slab geometry corresponding to $n = 2$ quadruplet layer (QL), we create an epitaxial heterostructures containing 2 unit cells of $CoCr_2O_4$ sandwitched between a ∼10 Å thick spacer layer of nonmagnetic and insulating $MgAl_2O_4$, as shown in Fig. S4. To minimize any magnetic interaction between the periodic images of $CoCr_2O_4$ slabs, the thickness of the $MgAl_2O_4$ spacer layer was chosen to be larger than the spin-correlation

length (6.0 Å) in bulk $CoCr_2O_4$. The $CoCr_2O_4/MgAl_2O_4$ heterostructure was optimized using the same convergence criteria as that for the bulk $CoCr_2O_4$, however, a relatively smaller Monkhorst-Pack type k-mesh of size $8 \times 8 \times 6$ was employed to sample the Brillouin zone. The Mg ($3s^2$) and Al ($3s^2 3p^1$) VASP PAW pseudo-potentials were used. The lattice parameters of optimized heterostructure are: $a = b = 5.82$ Å, and $c = 23.32$ Å ($\alpha = \gamma = 120°$, $\beta = 90°$).

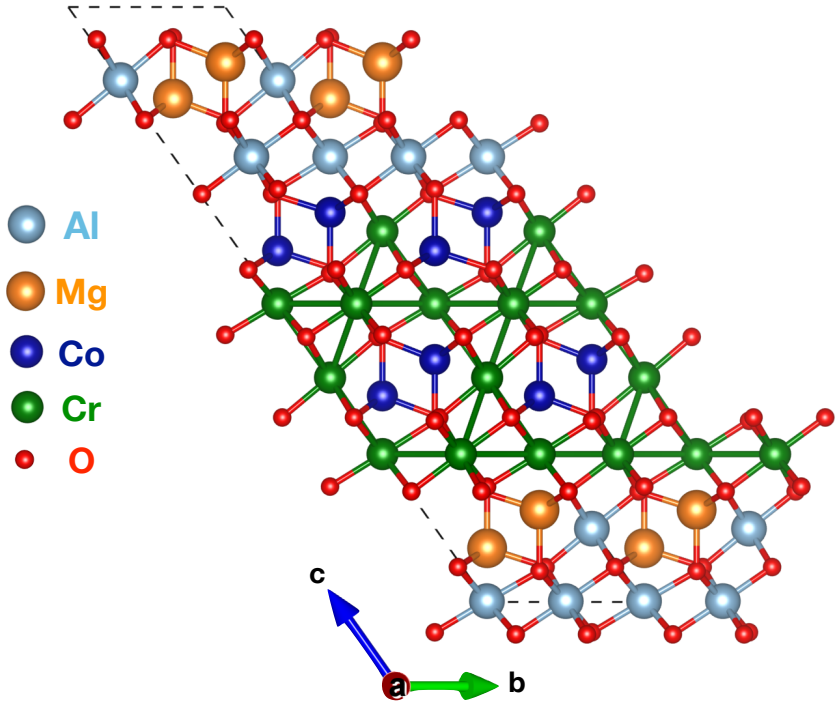

Figure S4: Side view of $n = 2$ QL epitaxial $CoCr_2O_4/MgAl_2O_4$ heterostructure.

Determination of magnetic exchange constants

To determine the magnetic exchange constants (J_{ij}) between the nearest (J^1_{ij}), and the next-nearest (J^2_{ij}) magnetic sites, we calculate the total energy of numerous different collinear magnetic configurations, and then project the DFT obtained total energies to a classical Heisenberg model,

$$E = \sum_{i,j} J^1_{ij} \vec{S}_i \cdot \vec{S}_j + \sum_{i',j'} J^2_{ij} \vec{S}_i \cdot \vec{S}_j \,. \tag{11}$$

Here, i, j indices refer to the nearest A (Co) and B (Cr) sublattices, whereas i', j' indices refer to the next-nearest A and B sublattices. In order to get the next-neighbour magnetic exchange terms in bulk, we used a doubled unit cell. However, no such doubling of unit cell was required for $n = 2$ QL $CoCr_2O_4/MgAl_2O_4$ heterostructure. The obtained values of magnetic exchange constants are listed in Table S2. Since J^1_{AA} is the weakest exchange at the first order in bulk $CoCr_2O_4$ (corresponding Co-Co bond length = 3.66 Å), we consider the J^2_{AA} to be negligible due to the large Co-Co bond length (∼6.0 Å) for the next neighbour Co-Co interactions.

Table S2: The nearest (J^1_{ij}), and the next-nearest (J^2_{ij}) magnetic exchange constants (in meV units) obtained using PBE+U for bulk $CoCr_2O_4$, and $n = 2$ QL $CoCr_2O_4/MgAl_2O_4$ heterostructure. The positive values denote antiferromagnetic (AFM) exchange interactions, whereas negative values denote ferromagnetic (FM) exchange interactions. The relative strength of each exchange interaction with respect to the most dominant J^1_{AB} is shown in the last two columns.

	bulk	$n = 2$	J^N_{ij}/J^1_{AB} (bulk)	J^N_{ij}/J^1_{AB} ($n = 2$)
J^1_{AB}	4.85	12.3	1	1
J^1_{BB}	2.10	6.35	0.43	0.52
J^1_{AA}	0.70	4.16	0.14	0.34
J^2_{AB}	-0.61	-1.03	-0.13	-0.08
J^2_{BB}	-0.04	-0.55	-0.01	-0.04

The obtained values of the nearest exchange interaction J^1_{ij} for bulk $CoCr_2O_4$ are in good agreement with the previous studies.[22,23,25,26] In bulk, J^1_{AB} is the leading exchange interaction which establishes the Néel type magnetic order in the system. Whereas, the subsequent J^1_{BB} and J^1_{AA} terms yield magnetic frustration at the A and B sites, respectively. A competition between J^1_{AB} and J^1_{BB} renders the spiral magnetic ordering in the bulk magnetic spinels. However, we note that the next-neighbor exchange interaction terms J^2_{ij} are FM in nature, therefore, the presence of the J^2_{ij} terms helps to counterbalance the magnetic frustration arising due to the AFM J^1_{ij}. Thus, a clear magnetic order establishes in the bulk system. In bulk $CoCr_2O_4$, our calculations reveal that J^2_{AB} is the most dominating exchange arising

from the next-nearest interactions, which is being followed by J^2_{BB} .

Comparing the strength of exchange terms in bulk and $n = 2$ cases, we notice a considerably large increase in the magnitude of J^1_{ij} and J^2_{ij}. In particular, J^1_{AA} increases by an order in magnitude. This is likely due to the fact that the overlap of atomic orbitals yielding magnetic exchanges changes when $CoCr_2O_4$ is confined between two nonmagnetic spacer layers. Major changes occur to the top Co layer at the $CoCr_2O_4$ and $MgAl_2O_4$ interface. As a result J^1_{AA} undergoes the maximum variation in a Co-terminated $CoCr_2O_4$ slab. Strikingly, the relative strength of J^1_{AA} (J^1_{AA}/J^1_{AB}) markedly increases from 0.14 to 0.34, whereas that of J^2_{AB} (J^2_{AB}/J^1_{AB}) decreases from 0.13 to 0.08. The same effect of enhanced magnetic frustration is generated from those two variations, which yields a Yafet-Kittel type magnetic ordering in the quasi-two dimensions.

References

(1) Liu, X.; Choudhury, D.; Cao, Y.; Middey, S.; Kareev, M.; Meyers, D.; Kim, J.-W.; Ryan, P.; Chakhalian, J. Epitaxial growth of (111)-oriented spinel $CoCr_2O_4/Al_2O_3$ heterostructures. *Appl. Phys. Lett.* **2015**, *106*, 071603(1–4).

(2) Thole, B. T.; Carra, P.; Sette, F.; van der Laan, G. X-ray circular dichroism as a probe of orbital magnetization. *Phys. Rev. Lett.* **1992**, *68*, 1943–1946.

(3) Carra, P.; Thole, B. T.; Altarelli, M.; Wang, X. X-ray circular dichroism and local magnetic fields. *Phys. Rev. Lett.* **1993**, *70*, 694–697.

(4) Corradini, V.; Moro, F.; Biagi, R.; del Pennino, U.; Renzi, V. D.; Carretta, S.; Santini, P.; Affronte, M.; Cezar, J. C.; Timco, G.; Winpenny, R. E. P. X-ray magnetic circular dichroism investigation of spin and orbital moments in Cr_8 and Cr_7Ni antiferromagnetic rings. *Phys. Rev. B* **2008**, *77*, 014402(1–8).

(5) Pathak, M.; Sims, H.; Chetry, K. B.; Mazumdar, D.; LeClair, P. R.; Mankey, G. J.;

Butler, W. H.; Gupta, A. Robust room-temperature magnetism of (110) CrO_2 thin films. *Phys. Rev. B* **2009**, *80*, 212405(1–4).

(6) Goering, E. X-ray magnetic circular dichroism sum rule correction for the light transition metals. *Philos. Mag.* **2005**, *85*, 2895–2911.

(7) Chen, C. T.; Idzerda, Y. U.; Lin, H. J.; Smith, N. V.; Meigs, G.; Chaban, E.; Ho, G. H.; Pellegrin, E.; Sette, F. Experimental confirmation of the x-ray magnetic circular dichroism sum rules for iron and cobalt. *Phys. Rev. Lett.* **1995**, *75*, 152–155.

(8) Goodenough, J. B. *Magnetism and the Chemical Bond*; Interscience: New York, 1974.

(9) Vonsovskii, S. V. *Magnetism Volume Two*; Wiley: New York, 1963.

(10) Kamenskyi, D.; Engelkamp, H.; Fischer, T.; Uhlarz, M.; Wosnitza, J.; Gorshunov, B. P.; Komandin, G. A.; Prokhorov, A. S.; Dressel, M.; Bush, A. A.; Torgashev, V. I.; Pronin, A. V. Observation of an intersublattice exchange magnon in $CoCr_2O_4$ and analysis of magnetic ordering. *Phys. Rev. B* **2013**, *87*, 134423(1–5).

(11) Altshuler, S. A.; Kozyrev, B. M. *Electron Paramagnetic Resonance in Compounds of Transition Elements*; Wiley: New York, 1974.

(12) Bercoff, P. G.; Bertorello, H. R. Exchange constants and transfer integrals of spinel ferrites. *J. Magn. Magn. Mater.* **1997**, *169*, 314–322.

(13) Guo, R.; Yu, Z.; Yang, Y.; Chen, L.; Sun, K.; Jiang, X.; Wu, C.; Lan, Z. Relationship between Curie temperature and Brillouin function characteristics of NiCuZn ferrites. *J. Appl. Phys.* **2015**, *117*, 073905(1–6).

(14) Guo, R.; Yu, Z.; Yang, Y.; Sun, K.; Wang, W.; Wu, C.; Jiang, X.; Liu, Y.; Lan, Z. Brillouin function for thermomagnetization characteristics of LiZnMn ferrites. *J. Appl. Phys.* **2017**, *4*, 016101(1–8).

(15) Singh, S.; Pramanik, P.; Sangaraju, S.; Mallick, A.; Giebeler, L.; Thota, S. Size-dependent structural, magnetic, and optical properties of $MnCo_2O_4$ nanocrystallites. *J. Appl. Phys.* **2017**, *121*, 194303(1–12).

(16) Blöchl, P. E. Projector augmented-wave method. *Phys. Rev. B* **1994**, *50*, 17953–17979.

(17) Kresse, G.; Joubert, D. From ultrasoft pseudopotentials to the projector augmented-wave method. *Phys. Rev. B* **1999**, *59*, 1758–1775.

(18) Kresse, G.; Furthmüller, J. Efficiency of ab-initio total energy calculations for metals and semiconductors using a plane-wave basis set. *Phys. Rev. B* **1996**, *54*, 11169–11186.

(19) Kresse, G.; Furthmüller, J. Efficient iterative schemes for ab initio total-energy calculations using a plane-wave basis set. *Comput. Mater. Sci.* **1996**, *6*, 15–50.

(20) Perdew, J. P.; Burke, K.; Ernzerhof, M. Generalized Gradient Approximation Made Simple. *Phys. Rev. Lett.* **1996**, *77*, 3865–3868.

(21) Dudarev, S. L.; Botton, G. A.; Savrasov, S. Y.; Humphreys, C. J.; Sutton, A. P. Electron-energy-loss spectra and the structural stability of nickel oxide: An LSDA+U study. *Phys. Rev. B* **1998**, *57*, 1505–1509.

(22) Efthimiopoulos, I.; Liu, Z. T. Y.; Khare, S. V.; Sarin, P.; Lochbiler, T.; Tsurkan, V.; Loidl, A.; Popov, D.; Wang, Y. Pressure-induced transition in the multiferroic $CoCr_2O_4$ spinel. *Phys. Rev. B* **2015**, *92*, 064108(1–9).

(23) Ederer, C.; Komelj, M. Magnetic coupling in $CoCr_2O_4$ and $MnCr_2O_4$: An LSDA + U stud. *Phys. Rev. B* **2007**, *76*, 064409(1–9).

(24) Wang, L.; Maxisch, T.; Ceder, G. Oxidation energies of transition metal oxides within the GGA + U framework. *Phys. Rev. B* **2006**, *73*, 195107(1–6).

(25) Lawes, G.; Melot, B.; Page, K.; Ederer, C.; Hayward, M. A.; Proffen, T.; Seshadri, R. Dielectric anomalies and spiral magnetic order in $CoCr_2O_4$. *Phys. Rev. B* **2006**, *74*, 024413(1–6).

(26) Heuver, J. A.; Scaramucci, A.; Blickenstorfer, Y.; Matzen, S.; Spaldin, N. A.; Ederer, C.; Noheda, B. Strain-induced magnetic anisotropy in epitaxial thin films of the spinel $CoCr_2O_4$. *Phys. Rev. B* **2015**, *92*, 214429(1–8).